Molecular and Cellular Neuroscience 123 (2022) 103772

Contents lists available at ScienceDirect

Molecular and Cellular Neuroscience

journal homepage: www.elsevier.com/locate/ymcne

Signal amplification in growth cone gradient sensing by a double negative feedback loop among PTEN, PI(3,4,5)P_3 and actomyosin

Xiong Li [a,b], Sangwoo Shim [a,b,c], Katherine R. Hardin [c], Kiran G. Vanaja [d], Hongjun Song [a,b,e,1], Andre Levchenko [d,2], Guo-li Ming [a,b,e,1,2], James Q. Zheng [c,*,2]

[a] Institute for Cell Engineering, Johns Hopkins University School of Medicine, 733 N. Broadway, Baltimore, MD 21205, USA
[b] Department of Neurology, Johns Hopkins University School of Medicine, 733 N. Broadway, Baltimore, MD 21205, USA
[c] Department of Cell Biology, Emory University School of Medicine, 615 Michael Street, Atlanta, GA 30322, USA
[d] Department of Biomedical Engineering and Yale Systems Biology Institute, Yale University, West Haven, CT 06516, USA
[e] The Solomon H. Snyder Department of Neuroscience, Johns Hopkins University School of Medicine, 725 N. Wolfe Street, Baltimore, MD 21205, USA

ARTICLE INFO

Keywords:
Axon guidance
Actin cytoskeleton
Chemotaxis
Phosphoinositide
Asymmetric signaling
Directional sensing

ABSTRACT

Axon guidance during neural wiring involves a series of precisely controlled chemotactic events by the motile axonal tip, the growth cone. A fundamental question is how neuronal growth cones make directional decisions in response to extremely shallow gradients of guidance cues with exquisite sensitivity. Here we report that nerve growth cones possess a signal amplification mechanism during gradient sensing process. In neuronal growth cones of *Xenopus* spinal neurons, phosphatidylinositol-3,4,5-trisphosphate (PIP_3), an important signaling molecule in chemotaxis, was actively recruited to the up-gradient side in response to an external gradient of brain-derived neurotrophic factor (BDNF), resulting in an intracellular gradient with approximate 30-fold amplification of the input. Furthermore, a reverse gradient of phosphatase and tensin homolog (PTEN) was induced by BDNF within the growth cone and the increased PTEN activity at the down-gradient side is required for the amplification of PIP_3 signals. Mechanistically, the establishment of both positive PIP_3 and reverse PTEN gradients depends on the filamentous actin network. Together with computational modeling, our results revealed a double negative feedback loop among PTEN, PIP_3 and actomyosin for signal amplification, which is essential for gradient sensing of neuronal growth cones in response to diffusible cues.

1. Introduction

Brain wiring requires guided extension of developing axons to their specific targets for synaptic connections (Kolodkin and Tessier-Lavigne, 2011; Tessier-Lavigne and Goodman, 1996). The motile tip of the axon, the growth cone, is equipped with an exquisite ability to sense a complex array of extracellular cues and to navigate through convoluted terrains of the developing brain. Evolutionally conserved families of guidance cues, either diffusible or surface-bound, are present in various temporal and spatial profiles during development to provide the directional instructions for elongating axons (Kolodkin and Tessier-Lavigne, 2011). Tremendous progress has been made in the past towards elucidating the molecular identities of guidance cues and their corresponding receptors (Bellon and Mann, 2018; Kolodkin and Tessier-Lavigne, 2011). The signaling and cellular events that translate various extracellular signals into specific responses of the growth cone have also been studied extensively (Gomez and Letourneau, 2014; Guy and Kamiguchi, 2021; Kerstein et al., 2015; Sánchez-Huertas and Herrera, 2021; Short et al., 2016; Vitriol and Zheng, 2012; Zang et al., 2021). However, the precise mechanisms by which a growth cone decodes the direction from the extracellular space during pathfinding have not been fully elucidated and many fundamental questions remain. In particular, diffusible guidance gradients *in vivo* are typically shallow with a steepness that is only a few percentages of the concentration of the guidance cue across a small growth cone (Sloan et al., 2015). Remarkably, it has been shown that, *in vitro*, a neuronal growth cone can detect a spatial heterogeneity

* Corresponding author.
E-mail address: james.zheng@emory.edu (J.Q. Zheng).
[1] Current address: Department of Neuroscience and Mahoney Institute for Neurosciences, Perelman School of Medicine, University of Pennsylvania, Philadelphia, PA, USA.
[2] Co-senior authors.

https://doi.org/10.1016/j.mcn.2022.103772
Received 1 June 2022; Received in revised form 23 August 2022; Accepted 26 August 2022
Available online 31 August 2022
1044-7431/© 2022 Elsevier Inc. All rights reserved.

of a guidance cue as small as 1 % over the growth cone's width (Mai et al., 2009; Rosoff et al., 2004; Wang et al., 2008), leading to highly polarized motile activities in the cytoskeletal, adhesion, and membranous dynamics for directed movement (Vitriol and Zheng, 2012). Such a high sensitivity suggests the existence of a signal amplification process along the signaling cascade relaying chemosensory information to biased neuronal growth cone behavior. Signal amplification and adaption are indispensable for chemotactic single cells, such as bacteria, amoebae and neutrophils, to respond to a wide dynamic range of chemoattractants with high sensitivity (Levchenko and Iglesias, 2002; SenGupta et al., 2021; Sourjik, 2004; Tu, 2013). In eukaryotic cells, phosphatidylinositol-3,4,5-trisphosphate (PIP_3) has been shown to play an important role in signal polarization during gradient sensing (Janetopoulos et al., 2004; Kolsch et al., 2008; Servant et al., 2000). PIP_3 is a second messenger and its level is dynamically regulated and tightly controlled through synthesis by phosphoinositide 3-kinase (PI3K) (Janetopoulos et al.) and degradation by phosphatase and tensin homolog (PTEN)/SH2-containing inositol phosphatase (SHIP) (Sun et al., 1999). PIP_3-dependent downstream signaling is initiated by its recruitment of pleckstrin homology (PH)-domain containing proteins, such as AKT kinases, to the plasma membrane. Previous studies have shown that PI3K/AKT and asymmetric PIP_3 are required for growth cone turning behavior to a gradient of guidance cues *in vitro* and *in vivo* (Henle et al., 2011; Ming et al., 1999). In this study, we investigated the signal amplification during gradient sensing by nerve growth cones. Using live cell imaging and computational modeling, we identified distinct roles of PIP_3, PTEN and actomyosin in amplifying guidance signals during growth cone navigation of *Xenopus* spinal neurons.

2. Methods

2.1. Reagents

BDNF was purchased from Peprotech (Rocky Hill, NJ). Cytochalasin B, latrunculin A, BDM were purchased from Sigma Chemicals (St. Louis, MO). Both bpV(pic) and bpV(HOpic) were purchased from ENZO Life Sciences (Plymouth Meeting, PA). Blebbistatin was purchased from EMD Chemicals (Gibbstown, NJ). All the inhibitors were bath applied to *Xenopus* neurons 20 min before the onset of BDNF pipette application.

2.2. Xenopus embryo injection and spinal neuron culture

GFP-PH_{AKT}, mCherry-PTEN, GFP-PTEN constructs were gifts from Dr. Peter Devreotes' lab (Johns Hopkins University, Baltimore, MD). The GFP-UtrCH construct was generously provided by Dr. William M. Bement (University of Wisconsin-Madison, Wisconsin). Blastomere injections of mRNAs encoding GFP-PH_{AKT}, mCherry-PTEN, GFP-PTEN or GFP-UtrCH into early stage *Xenopus* embryos and culturing of spinal neurons from these injected embryos were performed as previously described (Shim et al., 2005). Specifically, fertilized embryos were injected at the one- or two-cell stage, with a mixture of mRNA (2–3 ng/embryo) and the rhodamine-dextran (10KDa, Sigma). The following DNA constructs were subcloned into the pCS2 vector (gift of D. Turner, University of Michigan) and used for *in vitro* transcription with the mMESSAGE mMACHINE SP6 kit (Ambion, Austin, TX): GFP-PH_{AKT}, GFP-PTEN, mCherry-PTEN and GFP-UtrCH. The neurons ware cultured on custom glass-bottom dishes without coating. The cultures were incubated at room temperature (20 °C) for 16 h prior to the stimulation with either uniform BDNF or a BDNF gradient.

2.3. Stimulation with uniform BDNF or a BDNF gradient

For uniform stimulation, BDNF solution (125 ng/ml; final concentration) was added to the culture dish through pipetting. Micropipette system was used to generate the BDNF gradient as described previously (Lohof et al., 1992; Ming et al., 1997). Briefly, picoliter volumes of BDNF solution (100 μg/ml) were ejected to the culture through a micropipette with an opening of ~1 μm. The ejection was driven by repetitive pressure pulses of 3 psi in amplitude, 20 ms in duration and 2 Hz in frequency. The pressure was applied with an electrically gated pressure application system (Picospritzer, General Valve, Fairfield, NJ) and controlled using a pulse generator (SD9, Grass Instruments, Quincy, MA). During the turning assay, the pipette tip was placed 100 μm away from the growth cone with a 90-degree angle with regards to the extension direction of the distal 10 μm segment of the axon. For experiments with pharmacological inhibition, the drug was added to the cell culture media and incubated with the cells for 30 min prior to the experiments and remained in the culture during subsequent assays.

2.4. Fluorescent microscopy

The GFP or RFP fusion protein reporters and the rhodamine-dextran were imaged with a 63× Plan Fluor objective (NA 1.3 oil) on an inverted microscope (Axiovert, Zeiss) using a 488/512 nm and a 572/628 nm (ex/em) filter set, respectively. For each experiment, images of three channels (GFP, rhodamine and phase-contrast) were taken at 5 time points with a 1 min interval prior to stimulation. Fifteen minutes of recording was performed at 30 s intervals after the beginning of the stimulation. The Alexa Fluor 594 gradient was imaged with a 63× Plan Fluor objective (NA 1.3 oil) using a 572/628 nm (ex/em) filter.

2.5. Data analysis

The image processing was performed using the Image Processing Toolbox from MATLAB (Mathworks, Natick, MA). Background subtraction was carried out based on the measured intensity of pixels close to, but outside of, the growth cone. To quantify the changes of signals before and after stimulation, the outline of the growth cone palm was traced manually. The palm region of each growth cone was then divided into 6 equal-width domains. The average of GFP-PH_{AKT} to rhodamine ratio (F_{PH}) or GFP-PTEN to rhodamine ratio (F_{PTEN}) within each domain was calculated at every specified time point. The BDNF gradient was visualized and quantified in independent experiments by loading Alexa Fluor 594 dye together with BDNF into the micropipette tip. These measurements were then used to estimate the BDNF concentration at the periphery of the growth cone palm based on the distances of these pixels to the micropipette tip.

2.6. Mathematical model and simulation

To explore the interaction among PTEN, PI(3,4,5)P_3 and F-actin, we modeled the growth cone as a series of compartments, analogous to the experimental segmentation of the growth cones used in our experimental analysis. The active forms of PI3K (PI3K*) and PTEN (PTEN*), PI(4,5)P_2, PI(3,4,5)P_3, the membrane-bound PH-domain containing proteins (PH_m), dynamic F-actin (FActin) and actomyosin were membrane-bound species and thus were only present in the 'boundary compartments' corresponding to the compartment 1 and 6 in the experimental analysis. The inactive forms of PI3K and PTEN, actin monomer (GActin) and the unbound form of PH-domain containing proteins (PH) in both the membrane-cytosol interfaces and the cytosol and could diffuse freely within these spaces. In the model, this diffusion was accounted for by equivalent of the first Fick's law, describing the diffusive exchange at each interface between model compartments, proportional ot the difference of concentrations of a given species in these compartments. For instance, the concentration of PH in an intermediate (not boundary) model growth cone compartment i is described by the following equation:

$$\frac{dPH_i}{dt} = k_{ex}\,(PH_{i-1} - PH_i) + k_{ex}\,(PH_{i+1} - PH_i) = k_{ex}\Delta PH_{i,i-1} + k_{ex}\Delta PH_{i,i+1} \quad (1)$$

Similar equations describe the concentration dynamics for other diffusive species in the intermediate compartments.

The biochemical reactions are assumed to take place at the submembrane regions only, and are thus only modeled in the boundary compartments. The dynamics of the PTEN-PI(3,4,5)P_3-Dynamic F-actin-PTEN loop were described in Eqs. (2), (3), (4a), (5a), (6)–(12) and the dynamics of the PTEN-PI(3,4,5)P_3-Actomyosin-PTEN loop were described in Eqs. (2), (3), (4b), (5b), (6)–(12).

$$\frac{dPI3K}{dt} = kb_{PI3K} \bullet PI3K^* - kf_{PI3K} \bullet PI3K \bullet TrkB^* + k_{ex}\Delta PI3K \tag{2}$$

$$\frac{dPI3K^*}{dt} = kf_{PI3K} \bullet PI3K \bullet TrkB^* - kb_{PI3K} \bullet PI3K^* \tag{3}$$

$$\frac{dPTEN}{dt} = kb_{PTEN} \bullet PTEN^* - kf_{PTEN} \bullet PTEN \bullet FActin + k_{ex}\Delta PTEN \tag{4a}$$

$$\frac{dPTEN}{dt} = kb_{PTEN} \bullet PTEN^* - kf_{PTEN} \bullet PTEN \bullet Actomyosin + k_{ex}\Delta PTEN \tag{4b}$$

$$\frac{dPTEN^*}{dt} = kf_{PTEN} \bullet PTEN \bullet FActin - kb_{PTEN} \bullet PTEN^* \tag{5a}$$

$$\frac{dPTEN^*}{dt} = kf_{PTEN} \bullet PTEN \bullet Actomyosin - kb_{PTEN} \bullet PTEN^* \tag{5b}$$

$$\frac{dPIP2}{dt} = kb_{PIP_2} \bullet PIP_3 \bullet PTEN^* - kf_{PIP2} \bullet PIP_2 \bullet PI3K^* \tag{6}$$

$$\frac{dPIP3}{dt} = kf_{PIP2} \bullet PIP_2 \bullet PI3K^* - kb_{PIP_2} \bullet PIP_3 \bullet PTEN^* \tag{7}$$

$$\frac{dPH}{dt} = kb_{PH} \bullet PH_m - kf_{PH} \bullet PIP_3 \bullet PH + k_{ex}\Delta PH \tag{8}$$

$$\frac{dPH^*}{dt} = kf_{PH} \bullet PIP_3 \bullet PH - kb_{PH} \bullet PH_m \tag{9}$$

$$\frac{dGActin}{dt} = kb_{FActin} \bullet FActin + kb_{Actomyosin} \bullet Actomyosin - \left(kf_{FActin} \bullet PIP_3 + kf_{Actomyosin} \Big/ \left(km_{PIP_3} + PIP_3\right)\right) \bullet GActin + k_{ex}\Delta GActin \tag{10}$$

$$\frac{dGActin}{dt} = kf_{FActin} \bullet PIP_3 \bullet GActin - kb_{FActin} \bullet FActin \tag{11}$$

$$\frac{dActomyosin}{dt} = kf_{Actomyosin} \bullet GActin \Big/ \left(km_{PIP_3} + PIP_3\right) - kb_{Actomyosin} \bullet Actomyosin \tag{12}$$

In these equations the terms describing the diffusive exchange for some of the species are analogous to Eq. (1), relating the boundary and adjacent compartments.

The parameter values used in our simulation are listed in Table S1 and the initial conditions are listed in Table S2. The system input was the active Tropomyosin receptor kinase B (TrkB) receptor TrkB*. A 12.5 % TrkB* gradient was initiated between the growth cone's near and far sides at 5 min.

$$TrkB^* = 1, t < 300\ sec$$

$$\begin{cases} TrkB^* = 1.06, first\ comprtment \\ TrkB^* = 0.94, last\ compartment \end{cases} t \geq 300\ sec$$

The parameters were chosen to reproduce the kinetic behaviors seen in the experiments, with the diffusive exchange constant (k_{ex}) chosen in particular to model the reaction-limited rather than diffusion-limited cases. Assumptions of different values of the diffusive exchange constant for different molecular species did not strongly affect the results. The qualitative conclusions held under wide ranges of assumed parameter values.

3. Results

We have previously shown that an extracellular gradient of brain-derived neurotrophic factor (BDNF) can elicit robust attractive responses of *Xenopus* growth cones in culture (Ming et al., 1997). We therefore examined if growth cone sensing of the extracellular BDNF gradient involves PIP_3-based signaling and amplification. To directly visualize the dynamics of PIP_3 in neuronal growth cones, we expressed GFP-PH_{AKT} (PH-domain from AKT fused with GFP), a reporter of PIP_3 (Meili et al., 1999), in *Xenopus* embryonic spinal neurons. It should be noted that GFP-PH_{AKT} is also present in the cytosolic compartment and the cytosolic GFP-PH_{AKT} signal changes in association with growth cone volume and often overwhelms the membrane-bound GFP-PH_{AKT} signal. Therefore, we used rhodamine-dextran in the same cell as a volume marker to control for volume changes. The fluorescent ratio F_{PH} (GFP-PH_{AKT}/Rh-Dextran) is used to probe PIP3 and its changes. We found that a homogeneous bath application of BDNF (125 ng/ml) resulted in robust translocation and accumulation of GFP-PH_{AKT} at the edges of the growth cones as evidenced by increased F_{PH}, suggesting the active production of PIP_3 on the plasma membrane (Fig. 1). Consistent with previous results, BDNF also induced a rapid expansion of the lamellipodia (Ming et al., 1997).

We next examined the growth cone responses to a gradient of BDNF using a pipette application method (Lohof et al., 1992; Ming et al., 1997; Zheng et al., 1994). Consistent with previous reports, this pipette application method created a concentration gradient that became stable at 2 min after the onset of pressure ejection as assessed by the Alexa Fluor 594 fluorescence (Fig. S1). At 100 μm away from the pipette tip, the concentration gradient is relatively smooth and shallow, generating a fractional concentration change of ~10 % across a 10 μm distance (Lohof et al., 1992; Zheng et al., 1994). As a result, growth cone turning assays were typically performed by placing the pipette tip at 100 μm away from the growth cone and with a 45-degree angle to the direction of growth cone extension (Lohof et al., 1992; Ming et al., 1997; Zheng et al., 1994). In this study, we modified the pipette placement by placing the BDNF pipette at 100 μm away but in perpendicular to the direction of growth cone extension (*i.e.* with a 90-degree angle) to simplify the quantitative analysis of asymmetric growth cone signaling. Using GFP-PH_{AKT} to probe the spatiotemporal dynamics of PIP_3, we found that GFP-PH_{AKT} was preferentially recruited to the up-gradient side of the growth cone within 5 min (Fig. 2A-B). Intriguingly, we also observed a decrease of GFP-PH_{AKT} signal at the down-gradient side (Fig. 2A-B). No significant change in rhodamine-dextran signals was observed, indicating that the observed pattern of GFP-PH_{AKT} was not a result of volume changes of the growth cone but rather an asymmetric response to the BDNF gradient. Therefore, an extracellular BDNF gradient appears to have induced opposite changes in PIP_3 across the growth cone, generating a PIP3 asymmetry that may underlie growth cone turning towards the BDNF gradient.

To quantify the PIP_3 changes across the growth cone in response to a BDNF gradient using the volume normalized GFP-PH_{AKT} fluorescence (F_{PH}, see Fig. S2), we divided the palm region of the growth cones, including lamellipodia, into 6 equal-width domains, with domain 1 being farthest down-gradient while domain 6 nearest up-gradient (Fig. 2C). We then measured F_{PH} in each domain at various times before and after the onset of the BDNF gradient (before: −5, −1 min; after: 3, 5, 10 min). For each domain, the average of F_{PH} at −5 and − 1 min was used as the baseline signal (F_0) and changes in F_{PH} over times ($\Delta F_{PH}/F_0$) were calculated. We found that F_{PH} gradually increased in domain 6 after the onset of the BDNF gradient, resulting in an increase of 6.7 ± 2.9 % (n = 20) in $\Delta F_{PH}/F_0$ at 10 min after the onset of the BDNF gradient (Fig. 2C). Intriguingly, F_{PH} decreased in domain 1 in response

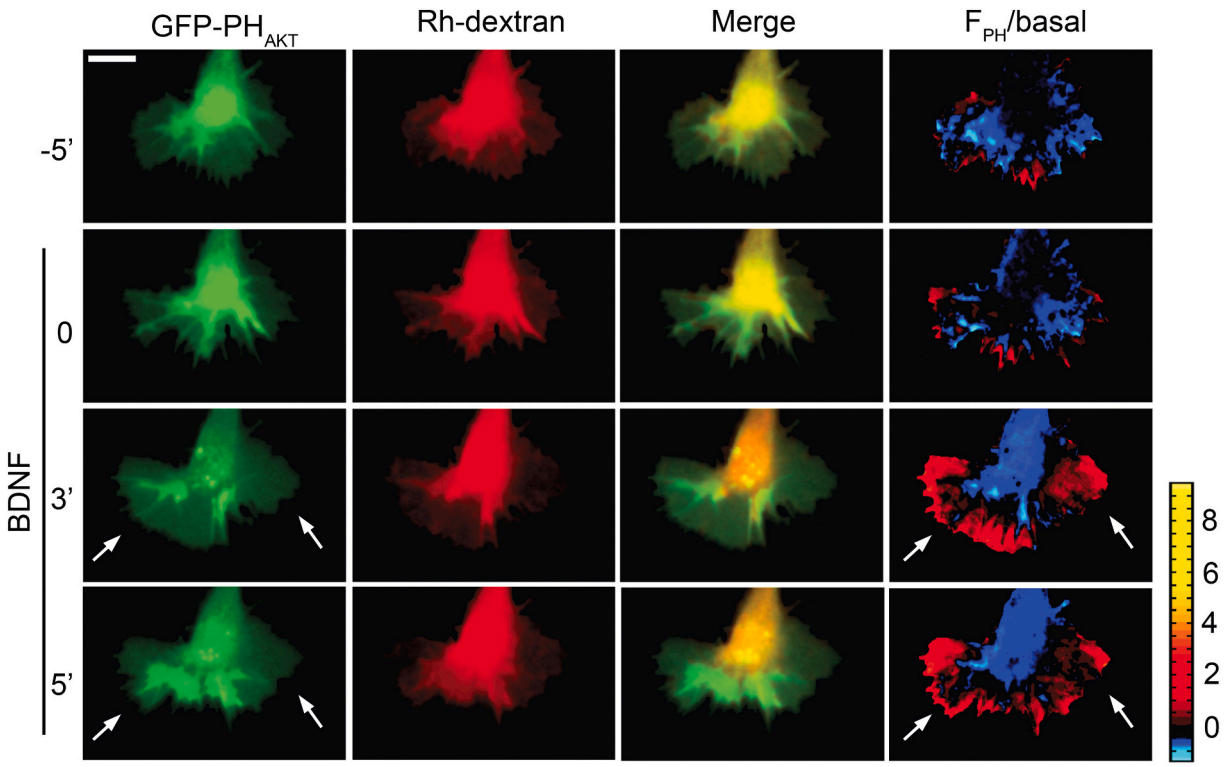

Fig. 1. Bath application of BDNF induces an elevation in PIP3 and results in lamellipodia protrusion. Representative fluorescent images of GFP-PH_{AKT} and Rhodamine-dextran (Rh-dextran) in a *Xenopus* growth cone at various times before and after the bath application of BDNF (125 ng/ml). The right column shows the corresponding pseudo-colored ratiometric images of GFP-PH_{AKT} to Rh-dextran (F_{PH}) normalized to its basal level (average F_{PH} of the growth cone at −5 and − 1 min). Arrows: expansion of lamellipodia. Scale bar: 5 μm.

to the BDNF gradient, resulting in a decrease of -4.9 ± 2.4 % in $\Delta F_{PH}/F_0$ at 10 min (Fig. 2C), suggesting an active mechanism in reducing the PIP_3 level at the down-gradient side. When $\Delta F_{PH}/F_0$ values across the growth cone at various times were plotted, it is evident that there is a gradient of $\Delta F_{PH}/F_0$ across the growth cone and, importantly, the steepness of the $\Delta F_{PH}/F_0$ gradient increases over time after the onset of the extracellular BDNF gradient (Fig. 2D).

To examine the input-output relationship between the imposed BDNF gradient and the responding intracellular PIP_3 gradient, we analyzed the slope of both extracellular BDNF gradients and the intracellular PIP3 asymmetry. For the extracellular BDNF gradient, we mixed BDNF with Alexa Fluor 594 (AF594) and performed fluorescent imaging at various times after the onset of the gradient application. Since the fluorescent signals measured here, especially volume-corrected GFP-PH_{AKT} signals (F_{PH}), do not represent the absolute concentrations of the molecule of interest, they cannot be directly used to calculate the concentration gradient and its slope. We therefore elected to use ΔF/F0 to assess the changes in the signal of interest (BDNF or PIP3) at a specific time point after the onset of pipette application of BDNF. For example, at 10 min after the onset of BDNF gradient, ΔF_{PH} equals to $F_{PH(10)} - F_{PH(0)}$ and $\Delta F_{PH}/F_{PH(0)}$ corresponds to the change in PIP3 signals after 10 min exposure to BDNF (Fig. S2). Since fractional changes (FC) are typically used to estimate the factional concentration gradient at a specific location (ΔC/C) (Sloan et al., 2015), we next calculated the fractional changes of the signal across the growth cone over its mean to determine the slope of the signal gradient (Fig. S2), similar to that previously described (Sloan et al., 2015). This analysis approach was also used to estimate the extracellular BDNF gradient across the growth cone by calculating the fractional changes of $\Delta F_{BDNF}/F_{BDNF(0)}$ (FC_{BDNF}) across the growth cone. Using this method, we found that the slope of FC_{BDNF} gradient over 10 μm distance at 100 μm away from the application pipette is about 9.9 ± 0.2 % (S.E.M, $n = 12$), which is consistent with the previous report (Lohof et al., 1992). The intracellular PIP_3 gradient as assessed by the fractional changes of $\Delta F_{PH}/F_0$, on the other hand, has a much steeper slope at 271.9 ± 64.9 % (S.E.M) over 10 μm, producing an approximately 33-fold amplification of the imposed BDNF gradient after 10 min BDNF exposure (Fig. 2E).

The reduction of PIP_3 at the down-gradient side of the growth cone in response to a BDNF gradient suggested a potential increase of a phosphoinositide phosphatase activity, either directly or indirectly. PTEN is known to be recruited to the membrane, and to reduce the PIP_3 level at the lagging side of *Dictyostelium* during chemotactic movements (Iijima and Devreotes, 2002). Thus, we examined the potential role of PTEN in gradient sensing of neuronal growth cones by expressing GFP-PTEN in *Xenopus* spinal neurons. Application of a BDNF gradient led to accumulation of GFP-PTEN at down-gradient side of growth cones within minutes (Fig. 3 A & B). At 10 min, ΔF_{PTEN} increased 2.9 ± 1.2 % ($n = 21$) in domain 1, but decreased 3.8 ± 1.1 % ($n = 21$) in domain 6 (Fig. 3C), resulting in an intracellular gradient in an opposite direction to the BDNF gradient (Fig. 3D). Calculation of the slope using the fractional changes of F_{PTEN} (FC_{PTEN}) at 10 min after the one of the BDNF yielded a slope of -202 ± 46 % (S.E.M) over 10 μm, which is about 25-fold amplification (Fig. 3E). To directly test the role of PTEN in PIP_3 signal amplification, we monitored the distribution of GFP-PH_{AKT} in response to a BDNF gradient in the presence of bpV(pic) or bpV(HOpic), two lipid phosphatase activity inhibitors of PTEN (Schmid et al., 2004). Bath application of either bpV(pic) or bpV(HOpic) alone induced an increase of GFP-PH_{AKT} at the plasma membrane (Fig. S3), suggesting that the basal level of PTEN activity under normal conditions acts to suppress the plasma membrane PIP_3 level. When growth cones were subjected to a BDNF gradient in the presence of either bpV(pic) or bpV(HOpic), the decrease of GFP-PH_{AKT} at the down-gradient side was converted to an increase, while the accumulation of GFP-PH_{AKT} at the up-gradient side was not affected, resulting in a complete loss of the intracellular PIP_3 gradient (Fig. 3F). Furthermore, application of bpV(pic) or bpV(HOpic) also abolished the attractive responses of growth cones to the BDNF

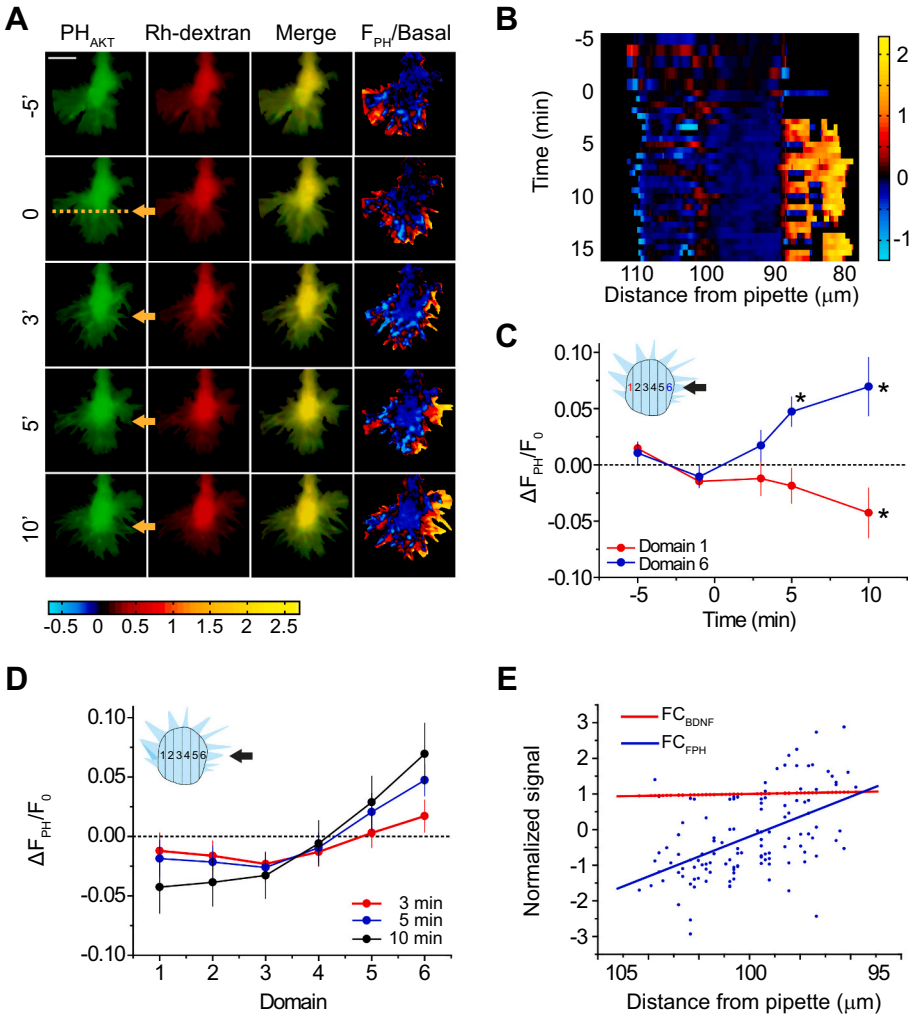

Fig. 2. An extracellular BDNF gradient induces an amplified PI(3,4,5)P_3 gradient within the growth cone. (A) Representative images of GFP-PH_{AKT} and Rh-dextran within a growth cone before and after the application of the BDNF gradient (the white arrow indicates the direction of the pipette tip). Ratiometric signal of GFP-PH_{AKT} to Rh-dextran (F_{PH}) was used as the final readout of PIP_3. The ratiometric images (right column) were resulted from F_{PH} images normalized to the basal average F_{PH} from the growth cone at −5 min and − 1 min. Scale bar: 5 μm. (B) The kymograph of normalized F_{PH} along the path that crosses the growth cone (indicated by the white line in (A) at time 0) in response to the BDNF gradient. (C) Application of the BDNF gradient induced an increase of ΔF_{PH} at the near side of the growth cones (Domain 6) and a decrease at the far side (Domain 1). Values represent mean ± SEM ($n = 20$; $^*P < 0.05$; Significantly different from that before onset of the gradient; Student's t-test). (D) The distribution of ΔF_{PH} within the 6 domains of the growth cones 3, 5 and 10 min after the application of the BDNF gradient. (E) Quantification of the imposed BDNF gradient and the responding ΔF_{PH} gradient suggested a 33 fold amplification from the input signal to the output. The distribution of BDNF levels and the changes of ΔF_{PH} within the 6 domains with regard to the distance from the pipette tip at 10 min in 20 growth cones, normalized to the means in each individual growth cone. The least-square fitted lines (red: ΔBDNF; blue: ΔF_{PH}) were computed using Matlab. (For interpretation of the references to color in this figure legend, the reader is referred to the web version of this article.)

gradient (Fig. 3G). Together, these results suggest that PTEN activity is essential for the amplification of the PIP_3 signal and growth cone steering.

The involvement of actin reorganization in polarized PIP_3 distribution is required for the chemotaxis of neutrophils, but not of *Dictyostelium* cells (Janetopoulos et al., 2004; Servant et al., 2000; Wang et al., 2002). We then asked whether actin polymerization is essential for signal amplification in growth cone guidance. Application of cytochalasin B (CB), a mycotoxin that binds to the barbed end of actin filaments to block actin polymerization, induced a loss of filopodia without collapsing the growth cones (Fig. S4A). Stimulation of CB treated neurons with a BDNF gradient induced an increase of GFP-PH_{AKT} at both the up-gradient side and the down-gradient side of the growth cones (Figs. 4A and S4B). Ten minutes after the gradient application, the ΔF_{PH} in domain 1 increased 5.8 ± 2.6 % ($n = 18$), similar to its increase in domain 6 (4.0 ± 2.0 %; Fig. 4 A & B). Importantly, the intracellular gradient of GFP-PH_{AKT} was essentially abolished in CB treated growth cones (slope = −72.4 ± 41.1 %). Application of latrunculin A (Lat A), a toxin sequestering actin monomers to prevent actin polymerization, showed similar results (Fig. 4B). Since inhibition of PTEN similarly affected the decrease of PIP_3 level at the down-gradient side, these results raised the possibility that actin polymerization might regulate the PTEN activity. To directly test this hypothesis, we examined the growth cones expressing GFP-PTEN in the presence of CB or Lat A. A BDNF gradient failed to induce an increase of PTEN levels at the far side of the growth cones (Fig. 4 C &D, Fig. S4 C&D); Instead, a reduction of PTEN levels was observed. After 10 min in the BDNF gradient, ΔF_{PTEN} in domain 1 decreased 3.5 ± 1.3 %, while that in domain 6 remained unchanged (−1.3 ± 1.5 %). These results suggest that actin polymerization is required for the amplification of PIP_3 during growth cone guidance through the regulation of PTEN localization.

There are two pools of actin structures within neuronal growth cones: the dynamic F-actin filaments with rapid disassembly and assembly, and the stable F-actin bundles coexisting with myosin (actomyosin) and with slower kinetics (Schaefer et al., 2002). PIP_3 could either promote the assembly of dynamic F-actin or interfere with the formation of the actomyosin structures (Xu et al., 2003). Our observation of the interaction between actin and PTEN suggests that PIP_3 and PTEN could form either a negative feedback loop involving reorganization of dynamic F-actin structures or a double negative (which is, in many ways, similar to a positive) feedback loop involving formation and function of actomyosin complexes (Fig. 5A). To assess which F-actin structure contributes to the amplification of PIP_3 during growth cone guidance, we developed two computational models to simulate the outcome of spatially graded stimulation of these two networks (Methods and Supplementary Data). In both models, the TrkB receptors, the active form of PI3K (PI3K*), the active form of PTEN (PTEN*), PIP_2, PIP_3, PIP_3-bound PH domain containing protein (PHm), dynamic F-actin (F-actin) and actomyosin were membrane-bound species, whereas the inactive forms of PI3K (PI3K), PTEN (PTEN), PH domain containing protein (PH) and the actin monomer (G-actin) were freely diffusible in the cytosol (Fig. 5B). When a 12.5 % BDNF gradient was imposed onto the simulated growth cone, the signaling network based on PTEN-PIP_3-Dynamic F-actin-PTEN negative feed-back loop failed to induce an amplification

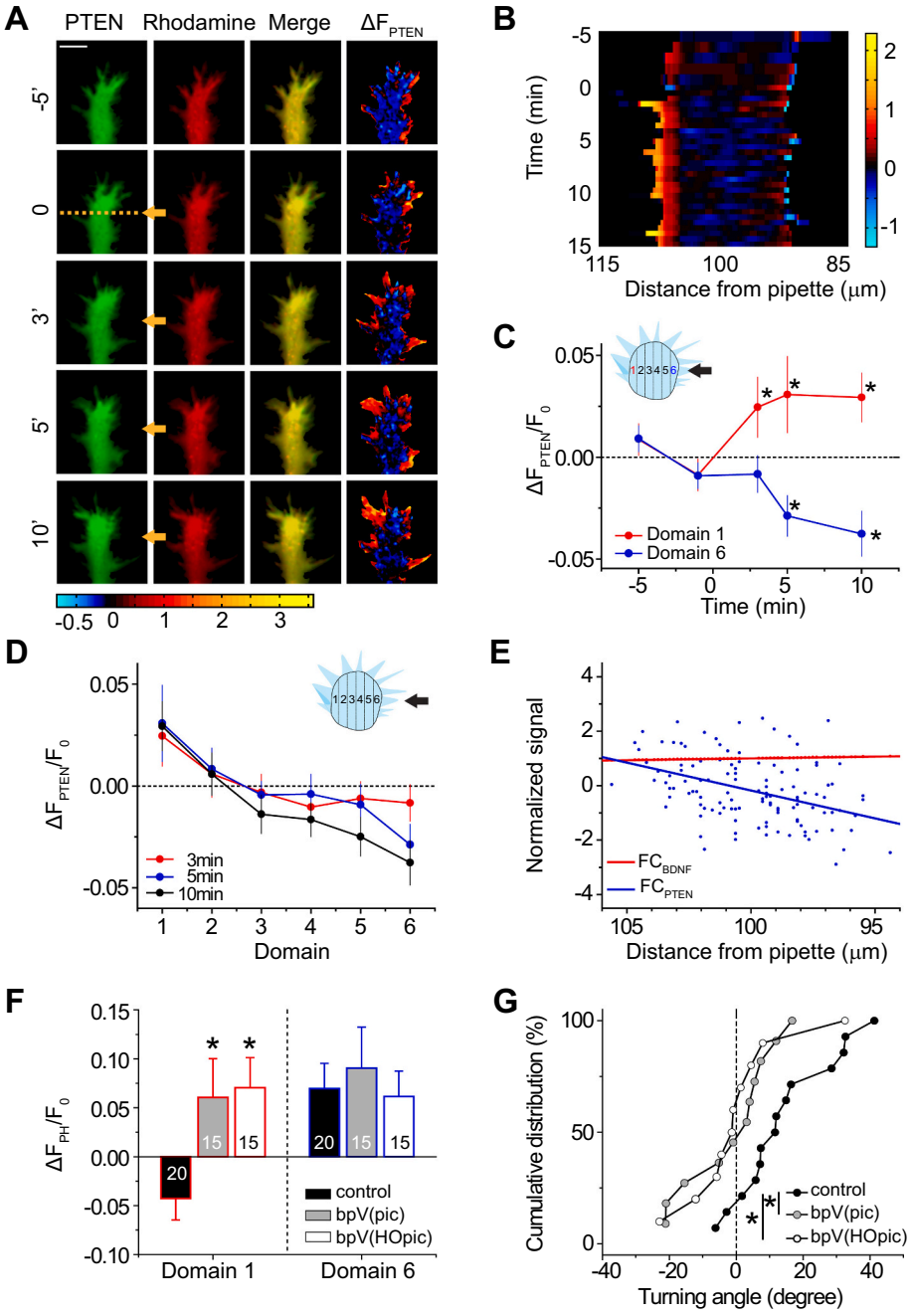

Fig. 3. Activation of PTEN mediates the inhibition of $PI(3,4,5)P_3$ production at the down-gradient side of the growth cones. (A) Sample images of GFP-PTEN and Rhodamine, and pseudo-color images of the normalized ratiometric signal ΔF_{PTEN} within a growth cone before and after the application of the BDNF gradient. Scale bar: 5 μm. (B) The kymograph of normalized ΔF_{PTEN} across the growth cone (indicated by the white line in (A) at time zero) in response to the BDNF gradient. (C) The application of the BDNF gradient induced a decrease of ΔF_{PTEN} signal at the near side of the growth cones (Domain 6), but an increase at the far side (Domain 1). Values represent mean ± SEM (n = 21; $^*P < 0.05$; Significantly different from that before onset of the gradient; Student's t-test). (D) The distribution of ΔF_{PTEN} within the 6 domains of the growth cone 3, 5 and 10 min after the application of the BDNF gradient. (E) The BDNF gradient induced an opposite ΔF_{PTEN} gradient with 25 fold amplification. Similar as in Fig. 1E, except that ΔF_{PTEN} was analyzed. (F) Inhibition of PTEN activity with bpV(pic) (5 μM) or bpV(HOpic) (5 μM) abolished the local inhibition of $PI(3,4,5)P_3$ at the down-gradient side of the growth cone. The number in the column is the total number of growth cones examined under each condition. Values represent mean ± SEM ($^*P < 0.05$; Student's t-test). (G) The application of bpV(pic) or bpV(HOpic) abolished attractive responses of growth cones to the BDNF gradient. Shown is a distribution plot of turning angles of individual neuronal growth cones at 30 min in the presence of a BDNF gradient under different treatments ($^*P < 0.05$; Kolmogorov-Smirnov test).

in PIP_3 (Fig. S5). In contrast, the model based on the PTEN-PIP_3-Actomyosin-PTEN double negative feedback loop predicted strongly amplified PIP_3 and PHm gradients, as well as a reversed PTEN gradient between the up- and down-gradient sides of the growth cone when the same BDNF gradient was applied (Fig. 5C, D). Importantly, the simulations also revealed that diffusion of inactive PI3K and PTEN within the simulated growth cone were crucial for the gradient amplification, by coupling the front and rear side of the growth cone (Fig. S5). The slope of the fractional PHm gradient was at least an order of magnitude steeper than the imposed BDNF gradient, similar to what we have observed in experimental settings. The model further predicted a slight elevation of actomyosin at the down-gradient side (2.5 %) and a 13.6 % reduction of actomyosin formation at the up-gradient side (Fig. 5E). Importantly, in this model, inhibition of PTEN activity or actin polymerization led to the abolishment of the amplification in PIP_3, which is also in agreement with our experimental observations (Fig. 5F). Together, the analyses suggested that the equivalent of a positive feedback involving PIP_3, PTEN and actomyosin coupled with diffusion of the signaling network components was sufficient to serve as the molecular basis for PIP_3 signal amplification in growth cone sensing. To test this prediction, we expressed the calponin homology (CH) domain of utrophin fused to GFP (GFP-UtrCH) in neurons, which selectively labeled stable actin filaments due to its slow binding dynamics with F-actin (Fig. S6A) (Burkel et al., 2007). As predicted by the simulation results, the intensity of GFP-UtrCH decreased at the up-gradient side of the growth cone upon BDNF stimulation (Fig. 5G, see also Fig. S6B). When GFP-UtrCH and mCherry-PTEN were co-expressed, the spatial correlation between these two fluorescent signals increased on the down-gradient side of the growth cones, indicating an increased co-localization of PTEN with actomyosin upon BDNF stimulation (Fig. 5H). Moreover, application of myosin ATPase inhibitors, 2,3-Butanedione monoxime (BDM) (Ostap, 2002) or Blebbistatin (Kovacs et al., 2004), abolished the increase of

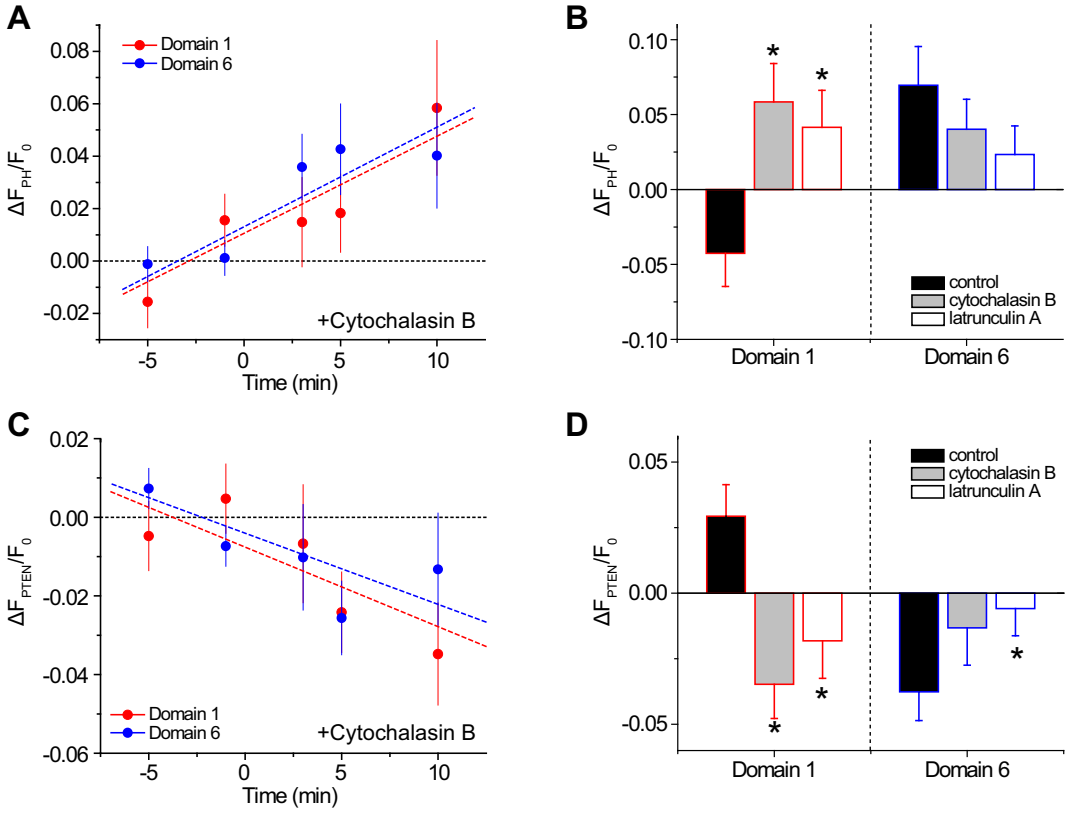

Fig. 4. Actin polymerization is required for establishing the amplified PI(3,4,5)P_3 and PTEN gradients in response to the BDNF gradient. (A) In the presence of cytochalasin B (7 μM), application of the BDNF gradient induced increases of ΔF_{PH} signal at both the near and far sides of growth cones. Values represent mean ± SEM ($n = 22$). Dot lines represent best linear fit. (B) Inhibition of actin polymerization with latrunculinA (100 nM) or cytochalasin B (7 μM) abolished the local inhibition of PIP_3 at the down-gradient side of the growth cones in the BDNF gradient. Values represent mean ± SEM (*$P < 0.05$; Student's *t*-test). (C) In the presence of cytochalasin B, the application of the BDNF gradient induced slight decreases of ΔF_{PTEN} at both the near and far sides of the growth cones. Values represent mean ± SEM ($n = 21$). Dot lines represent best linear fit. (D) Inhibition of actin polymerization with cytochalasin B or latrunculin A abolished both the accumulation of PTEN at the down-gradient side and decreased PTEN localization at the up-gradient side within the growth cones in the BDNF gradient. Values represent mean ± SEM (*$P < 0.05$; Student's t-test).

PTEN and its co-localization with actomyosin (Fig. 5I). While the specific myosin members cannot be determined by these two inhibitors, these results suggest that interaction with actomyosin is required for the accumulation and activation of PTEN at the down-gradient side of the growth cone in response to a BDNF gradient. Together with computational modeling, our results support a double negative feedback loop with diffusive components for PIP_3 signal amplification in growth cone gradient sensing.

4. Discussion

The cell or growth cone's ability to sense the environment and to determine the direction and proximity of an extracellular stimulus, followed by correct movement, is fundamental not only for neural development (*e.g.* neuronal migration and growth cone guidance) but also for immunity, angiogenesis, wound healing, and embryogenesis. Chemotaxis is an important feature employed by many cells to gain directional movement that is essential for their survival and function. While bacteria use random walk to move up and down a diffusible gradient, large cells such as amoebae and lymphocytes are equipped with the ability to detect the concentration difference of extracellular cues across their surface and, importantly, translate it into actin-based directional motility. It has been shown that chemotactic cells can detect shallow extracellular gradients with a relative concentration steepness as low as 2 % between the front and the back of the cell (Parent and Devreotes, 1999). To achieve this task, a signal amplification mechanism has been proposed that can generate a much steeper gradient of intracellular responses, leading to highly polarized actin-based activities required for directed cell movement (Jin, 2013; Levchenko and Iglesias, 2002; SenGupta et al., 2021). Nerve growth cones in vertebrate have an average size of ~5–10 μm and they are known to be capable of responding to shallow guidance gradients with a steepness of as low as 1 % *in vitro* and *in vivo* (Mai et al., 2009; Rosoff et al., 2004; Sloan et al., 2015; Wang et al., 2008). Imaging studies have shown that directional responses of nerve growth cones involve highly polarized motile activities including preferential actin-based protrusion, membrane recycling, and dynamic modification of adhesion (Vitriol and Zheng, 2012). Therefore, the tiny concentration difference of the guidance cues between the "near" (up-gradient) and "far" (down-gradient) sides of the growth cone is able to elicit highly asymmetric motile activities, suggesting the existence of signal amplification. However, no detailed investigation has been performed to examine the signal amplification and its underlying mechanism during growth cone guidance.

Several molecular species or chemical processes have been shown to display a polarized distribution during growth cone guidance, including gamma amino-butyric acid (GABA) receptors, inositol 1,4,5-triphsphate (IP_3), PIP_3, mRNAs for β-actin, membrane transportation and exocytosis (Akiyama et al., 2009; Bouzigues et al., 2007; Henle et al., 2011; Hevroni et al., 1998; Leung et al., 2006; Quinn et al., 2008; Tojima et al., 2007; Yao et al., 2006). It was also reported that activated Src family kinase (pSrc) exhibited a polarized distribution in the growth cone only when two shallow gradients of netrin-1 and sonic hedgehog (Shh) proteins were combined (Sloan et al., 2015). Interestingly, the combined shallow

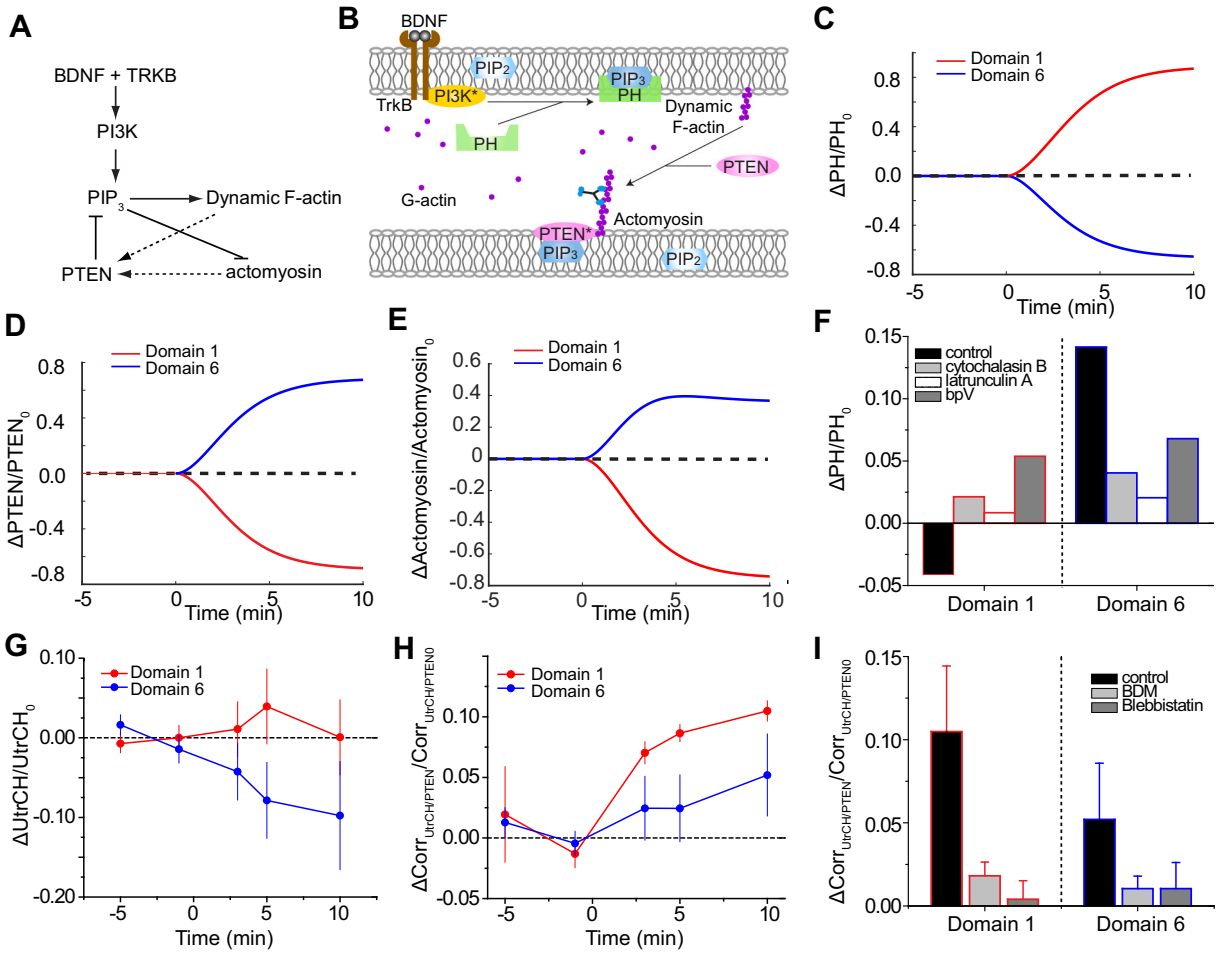

Fig. 5. Integrated analyses with computational modeling and live imaging suggest that positive feedback among PTEN, PI(3,4,5)P_3 and actomyosin function as the molecular basis for PI(3,4,5)P_3 amplification. (A) Diagrams describing potential feedback interactions between PTEN and PIP_3 through either dynamic F-actin or actomyosin. (B) Schematic of the distributions of signaling molecules at growth cone's membrane and cytosol assumed in the model. (C-E) Simulated responses of the membrane-bound PH-domain containing proteins (C), activated PTEN (D) and actomyosin structures (E) at the near or far sides of the growth cone in the BDNF gradient based on the PTEN-PI(3,4,5)P_3-actomyosin-PTEN feedback. Please see Supplementary Materials for equations and details. (F) Simulation of the effects of Cytochalasin B, Latrunculin A or bpV on PI(3,4,5)P_3 polarization. (G) Stable F-actin visualized by GFP-UtrCH displayed a decrease at the near side of the growth cone following BDNF gradient stimulation. Values represent mean ± SEM. (H) The spatial correlation between GFP-UtrCH and mCherry-PTEN increased at the far side of the growth cones. (I) Application of myosine ATPase inhibitors, BDM or Blebbistatin, abolished the increased correlation between GFP-UtrCH and mCherry-PTEN in the BDNF gradient. Values represent mean ± SEM.

netrin-1 and Shh gradients (~1 % fractional changes each) resulted in an approximately a ~ 15 % fractional change in pSrc across the growth cone, suggesting an amplification. Our work presented here is the first demonstration of a substantial amplification of the input gradient signal during growth cone gradient sensing. Our finding that a gradient of guidance molecule induces a positive PIP_3 gradient and an opposing negative PTEN gradient is consistent with previous studies in chemotactic neutrophil cells, suggesting a conservation of signaling events underlying chemotaxis in different systems. Interestingly, the internal gradients of PIP_3 exhibited an approximately 33-fold amplification of the imposed BDNF external gradient, an amplitude that is much larger than those reported for *Dictyostelium* (8-fold) (Janetopoulos et al., 2004) and neutrophils (6-fold) (Servant et al., 2000), indicating a much greater sensitivity of neuronal growth cones. By integrating computational modeling and live fluorescence imaging, we demonstrated that this remarkable sensitivity of growth cone gradient detection could be attributed to a positive feedback through PTEN, PIP_3 and actomyosin. We found that the accumulation of PTEN at the far side of a growth cone requires actomyosin-mediated transportation, in line with a recent study demonstrating that the activation of PTEN in neurons is dependent on actin and myosin-based transportation to the plasma membrane (van Diepen et al., 2009). The connection between actomyosin and PTEN activation completes the double negative feedback loop among PTEN, PIP_3 and actomyosin, which along with the key requirement of cross-growth cone diffusion or active transport of the network components, constitutes the underlying mechanism for signal amplification in growth cone guidance. In contrast, in the chemotaxis of amoebae, actin polymerization is not required for signal amplification and there is no pronounced amplification of the PTEN gradient in response to an extracellular cAMP gradient (*7*). In neutrophil chemotaxis, actin is required for signal amplification but PTEN does not seem to play a major role in this process (*6*). Thus, our studies suggest that the double negative feedback loop (similar in many ways to a positive feedback loop frequently leading to switch-like responses), involving PTEN, PIP_3 and actomyosin lies at the core of distinctive mechanism that accounts for the ultra-sensitivity in growth cone gradient response.

CRediT authorship contribution statement

X.L., A. L., and G-l. M. designed the initial research; X. L. and S. S. performed research and analyzed most of the data; X.L., K.G.V. and A. L. developed the mathematical model; K.R.H. performed additional

analysis on the BDNF gradient. H.S. contributed to the data interpretation and discussion. J. Q. Z. helped the further development of the research, contributed new reagents, performed new data analysis, and revised the manuscript; X.L., G-l. M, A.L., and J.Q.Z. wrote the paper and its revisions.

Declaration of competing interest

The authors declare that they have no competing financial interests.

Acknowledgments

We thank Drs. P. Devreotes and W.M. Bement for reporter constructs, L. Liu and Y. Cai for technical support. This work was supported in part by NIH research grants to G-L.M. (NS048271, HD069184), A.L (CA209992) and J.Q.Z. (GM083889).

Appendix A. Supplementary data

Supplementary data to this article can be found online at https://doi.org/10.1016/j.mcn.2022.103772.

References

Akiyama, H., Matsu-ura, T., Mikoshiba, K., Kamiguchi, H., 2009. Control of neuronal growth cone navigation by asymmetric inositol 1,4,5-trisphosphate signals. Sci. Signal. 2, ra34.
Bellon, A., Mann, F., 2018. Keeping up with advances in axon guidance. Curr. Opin. Neurobiol. 53, 183–191.
Bouzigues, C., Morel, M., Triller, A., Dahan, M., 2007. Asymmetric redistribution of GABA receptors during GABA gradient sensing by nerve growth cones analyzed by single quantum dot imaging. Proc. Natl. Acad. Sci. U. S. A. 104, 11251–11256.
Burkel, B.M., von Dassow, G., Bement, W.M., 2007. Versatile fluorescent probes for actin filaments based on the actin-binding domain of utrophin. Cell Motil. Cytoskeleton 64, 822–832.
van Diepen, M.T., Parsons, M., Downes, C.P., Leslie, N.R., Hindges, R., Eickholt, B.J., 2009. MyosinV controls PTEN function and neuronal cell size. Nat. Cell Biol. 11, 1191–1196.
Gomez, T.M., Letourneau, P.C., 2014. Actin dynamics in growth cone motility and navigation. J. Neurochem. 129, 221–234.
Guy, A.T., Kamiguchi, H., 2021. Lipids as new players in axon guidance and circuit development. Curr. Opin. Neurobiol. 66, 22–29.
Henle, S.J., Wang, G., Liang, E., Wu, M., Poo, M.M., Henley, J.R., 2011. Asymmetric PI (3,4,5)P3 and akt signaling mediates chemotaxis of axonal growth cones. J. Neurosci. 31, 7016–7027.
Hevroni, D., Rattner, A., Bundman, M., Lederfein, D., Gabarah, A., Mangelus, M., Silverman, M.A., Kedar, H., Naor, C., Kornuc, M., Hanoch, T., Seger, R., Theill, L.E., Nedivi, E., Richter-Levin, G., Citri, Y., 1998. Hippocampal plasticity involves extensive gene induction and multiple cellular mechanisms. J. Mol. Neurosci. 10, 75–98.
Iijima, M., Devreotes, P., 2002. Tumor suppressor PTEN mediates sensing of chemoattractant gradients. Cell 109, 599–610.
Janetopoulos, C., Ma, L., Devreotes, P.N., Iglesias, P.A., 2004. Chemoattractant-induced phosphatidylinositol 3,4,5-trisphosphate accumulation is spatially amplified and adapts, independent of the actin cytoskeleton. Proc. Natl. Acad. Sci. U. S. A. 101, 8951–8956.
Jin, T., 2013. Gradient sensing during chemotaxis. Curr. Opin. Cell Biol. 25, 532–537.
Kerstein, P.C., Nichol, R.H.T., Gomez, T.M., 2015. Mechanochemical regulation of growth cone motility. Front. Cell. Neurosci. 9, 244.
Kolodkin, A.L., Tessier-Lavigne, M., 2011. Mechanisms and molecules of neuronal wiring: a primer. Cold Spring Harb. Perspect. Biol. 3.
Kolsch, V., Charest, P.G., Firtel, R.A., 2008. The regulation of cell motility and chemotaxis by phospholipid signaling. J. Cell Sci. 121, 551–559.
Kovacs, M., Toth, J., Hetenyi, C., Malnasi-Csizmadia, A., Sellers, J.R., 2004. Mechanism of blebbistatin inhibition of myosin II. J. Biol. Chem. 279, 35557–35563.
Leung, K.M., van Horck, F.P., Lin, A.C., Allison, R., Standart, N., Holt, C.E., 2006. Asymmetrical beta-actin mRNA translation in growth cones mediates attractive turning to netrin-1. Nat. Neurosci. 9, 1247–1256.
Levchenko, A., Iglesias, P.A., 2002. Models of eukaryotic gradient sensing: application to chemotaxis of amoebae and neutrophils. Biophys. J. 82, 50–63.
Lohof, A.M., Quillan, M., Dan, Y., Poo, M.M., 1992. Asymmetric modulation of cytosolic cAMP activity induces growth cone turning. J. Neurosci. 12, 1253–1261.
Mai, J., Fok, L., Gao, H., Zhang, X., Poo, M.M., 2009. Axon initiation and growth cone turning on bound protein gradients. J. Neurosci. 29, 7450–7458.
Meili, R., Ellsworth, C., Lee, S., Reddy, T.B., Ma, H., Firtel, R.A., 1999. Chemoattractant-mediated transient activation and membrane localization of Akt/PKB is required for efficient chemotaxis to cAMP in dictyostelium. EMBO J. 18, 2092–2105.
Ming, G., Lohof, A.M., Zheng, J.Q., 1997. Acute morphogenic and chemotropic effects of neurotrophins on cultured embryonic xenopus spinal neurons. J. Neurosci. 17, 7860–7871.
Ming, G., Song, H., Berninger, B., Inagaki, N., Tessier-Lavigne, M., Poo, M., 1999. Phospholipase C-gamma and phosphoinositide 3-kinase mediate cytoplasmic signaling in nerve growth cone guidance. Neuron 23, 139–148.
Ostap, E.M., 2002. 2,3-butanedione monoxime (BDM) as a myosin inhibitor. J. Muscle Res. Cell Motil. 23, 305–308.
Parent, C.A., Devreotes, P.N., 1999. A cell's sense of direction. Science 284, 765–770.
Quinn, C.C., Pfeil, D.S., Wadsworth, W.G., 2008. CED-10/Rac1 mediates axon guidance by regulating the asymmetric distribution of MIG-10/lamellipodin. Curr. Biol. 18, 808–813.
Rosoff, W.J., Urbach, J.S., Esrick, M.A., McAllister, R.G., Richards, L.J., Goodhill, G.J., 2004. A new chemotaxis assay shows the extreme sensitivity of axons to molecular gradients. Nat. Neurosci. 7, 678–682.
Sánchez-Huertas, C., Herrera, E., 2021. With the permission of microtubules: an updated overview on microtubule function during axon pathfinding. Front. Mol. Neurosci. 14, 759404.
Schaefer, A.W., Kabir, N., Forscher, P., 2002. Filopodia and actin arcs guide the assembly and transport of two populations of microtubules with unique dynamic parameters in neuronal growth cones. J. Cell Biol. 158, 139–152.
Schmid, A.C., Byrne, R.D., Vilar, R., Woscholski, R., 2004. Bisperoxovanadium compounds are potent PTEN inhibitors. FEBS Lett. 566, 35–38.
SenGupta, S., Parent, C.A., Bear, J.E., 2021. The principles of directed cell migration. Nat. Rev. Mol. Cell Biol. 22, 529–547.
Servant, G., Weiner, O.D., Herzmark, P., Balla, T., Sedat, J.W., Bourne, H.R., 2000. Polarization of chemoattractant receptor signaling during neutrophil chemotaxis. Science 287, 1037–1040.
Shim, S., Goh, E.L., Ge, S., Sailor, K., Yuan, J.P., Roderick, H.L., Bootman, M.D., Worley, P.F., Song, H., Ming, G.L., 2005. XTRPC1-dependent chemotropic guidance of neuronal growth cones. Nat. Neurosci. 8, 730–735.
Short, C.A., Suarez-Zayas, E.A., Gomez, T.M., 2016. Cell adhesion and invasion mechanisms that guide developing axons. Curr. Opin. Neurobiol. 39, 77–85.
Sloan, T.F., Qasaimeh, M.A., Juncker, D., Yam, P.T., Charron, F., 2015. Integration of shallow gradients of shh and Netrin-1 guides commissural axons. PLoS Biol. 13, e1002119.
Sourjik, V., 2004. Receptor clustering and signal processing in E. Coli chemotaxis. Trends Microbiol. 12, 569–576.
Sun, H., Lesche, R., Li, D.M., Liliental, J., Zhang, H., Gao, J., Gavrilova, N., Mueller, B., Liu, X., Wu, H., 1999. PTEN modulates cell cycle progression and cell survival by regulating phosphatidylinositol 3,4,5,-trisphosphate and Akt/protein kinase B signaling pathway. Proc. Natl. Acad. Sci. U. S. A. 96, 6199–6204.
Tessier-Lavigne, M., Goodman, C.S., 1996. The molecular biology of axon guidance. Science 274, 1123–1133.
Tojima, T., Akiyama, H., Itofusa, R., Li, Y., Katayama, H., Miyawaki, A., Kamiguchi, H., 2007. Attractive axon guidance involves asymmetric membrane transport and exocytosis in the growth cone. Nat. Neurosci. 10, 58–66.
Tu, Y., 2013. Quantitative modeling of bacterial chemotaxis: signal amplification and accurate adaptation. Annu. Rev. Biophys. 42, 337–359.
Vitriol, E.A., Zheng, J.Q., 2012. Growth cone travel in space and time: the cellular ensemble of cytoskeleton, adhesion, and membrane. Neuron 73, 1068–1081.
Wang, F., Herzmark, P., Weiner, O.D., Srinivasan, S., Servant, G., Bourne, H.R., 2002. Lipid products of PI(3)Ks maintain persistent cell polarity and directed motility in neutrophils. Nat. Cell Biol. 4, 513–518.
Wang, C.J., Li, X., Lin, B., Shim, S., Ming, G.L., Levchenko, A., 2008. A microfluidics-based turning assay reveals complex growth cone responses to integrated gradients of substrate-bound ECM molecules and diffusible guidance cues. Lab Chip 8, 227–237.
Xu, J., Wang, F., Van Keymeulen, A., Herzmark, P., Straight, A., Kelly, K., Takuwa, Y., Sugimoto, N., Mitchison, T., Bourne, H.R., 2003. Divergent signals and cytoskeletal assemblies regulate self-organizing polarity in neutrophils. Cell 114, 201–214.
Yao, J., Sasaki, Y., Wen, Z., Bassell, G.J., Zheng, J.Q., 2006. An essential role for beta-actin mRNA localization and translation in Ca2+-dependent growth cone guidance. Nat. Neurosci. 9, 1265–1273.
Zang, Y., Chaudhari, K., Bashaw, G.J., 2021. New insights into the molecular mechanisms of axon guidance receptor regulation and signaling. Curr. Top. Dev. Biol. 142, 147–196.
Zheng, J.Q., Felder, M., Connor, J.A., Poo, M.M., 1994. Turning of nerve growth cones induced by neurotransmitters. Nature 368, 140–144.